Estimation of Mesoscale Vertical Derivatives of Potential Temperature and Density from Hydrographic Data

ARTHUR J. MARIANO

Department of Applied Science, Harvard University, Cambridge, Massachusetts

(Manuscript received 4 August 1987, in final form 15 June 1989)

ABSTRACT

This study was motivated by the need to combine vertical derivative estimates of either potential density or temperature with SOFAR float data for estimating vortex stretching in the main (700 m) and lower thermocline (1300 m) of the Local Dynamics Experiment (LDE) region. Five hundred, forty-three LDE CTD casts are used to evaluate finite difference, polynomial and exponential regression models for estimating the mesoscale vertical derivative of potential density and temperature at 700 and 1300 m depth. The standard deviation and bias curves of these models were examined as a function of vertical estimation interval. Smoothing the data before derivative estimation was not necessary for estimation intervals greater than 300 m for all the models tested. An unbiased minimum variance estimator of vertical derivatives does not exist for the models tested because of a variance-bias trade-off.

An alternate criterion of merit is proposed for the estimation of vertical derivatives: We require that vortex stretching estimates be robust to small changes in the estimation interval and that the vortex stretching estimates agree with the estimates of Mariano and Rossby. According to this criterion, a cubic polynomial fit of length 800 ± 100 m to the density data is the *best* model for estimating vertical derivatives from hydrographic data at 700 m. Because the stretching is less at 1300 m and uncertainties are great, vortex stretching could not be estimated using this approach with sufficient accuracy at 1300 m.

1. Introduction

Vertical derivatives of potential temperature and potential density are fundamental dynamical quantities that are estimated from hydrographic data. *Good* estimates of these vertical derivatives and error bounds of those estimates are needed in the study of many important oceanic research problems. One of these is the study of mesoscale dynamics using the potential vorticity equation.

For mesoscale processes, the product of the planetary vorticity, f, and the material derivative of the natural log of the vertical derivative of potential density or potential temperature is a very good approximation to the stretching term in the Lagrangian formulation of Ertel's potential vorticity equation (Mariano and Rossby 1989, hereafter MR89),

$$\text{vortex stretching} = f * \left(d/dt \left[\ln\left(\frac{\partial \lambda}{\partial z} \right) \right] \right), \quad (1.1)$$

where λ is either potential temperature or potential density. The following experiment was designed to investigate how well one can estimate the vortex stretching term using (1.1) by calculating the material time derivative from estimates of $\partial\rho/\partial z$ or $\partial\theta/\partial z$ based on hydrographic profiles along SOFAR float trajectories.

In the POLYMODE Local Dynamics Experiment (LDE) region, a 250 × 250 km region centered on 31.0°N, 69.5°W, numerous SOFAR floats were released at 700 and 1300 m to study the evolution of the mesoscale eddy field (Rossby et al. 1986). Shore-based receivers provided real time tracking of SOFAR floats and enabled scientists aboard R/V *Gyre* cruise G-6-78 to take salinity–temperature–depth (STD) profiles very close to SOFAR float trajectories. Preliminary analysis of the float and hydrographic data, with the vertical derivative of potential density approximated by a finite difference of 100 m length, yielded stretching estimates an order of magnitude too large, despite pairs of STD profiles that, to a good approximation, followed particle trajectories.

The horizontal sampling error, which is due to a combination of hydrocasts not exactly on particle trajectories and error in estimating the particle trajectories from constant pressure SOFAR float position data, cannot be addressed with the given data set, but it is probably small. The SOFAR float position and velocity data has been filtered with a low-pass Gaussian filter with a half-power point at 2½ days to remove submesoscale noise. Most of the float position data error, which remains after filtering, is highly correlated (Spain et al. 1980) and is removed by the temporal difference in (1.1). It appears that most of the error in the stretch-

Corresponding author address: Dr. Arthur Mariano, RSMAS/MPO, University of Miami, 4600 Rickenbacker Causeway, Miami, FL 33149-1098.

ing estimates is due to the estimation of the vertical derivative in (1.1). The objective of this paper is to investigate different models for estimating the mesoscale vertical derivative from hydrographic data.

Specifically, three common vertical derivative models and different estimation intervals are tested to see how well one can estimate the mesoscale vertical derivative of potential temperature and potential density from hydrographic data. The evaluation and discussion of the derivative models focuses on the vertical derivative of potential temperature, so that the results can be extended to XBT data. The test results for temperature and density are similar and the important differences are noted. The derivative models are evaluated for a range of symmetric estimation intervals; 20 to 1200 m for the 700 m floats and 20 to 2400 m for the 1300 m floats. Five hundred, forty-three CTD profiles, from the intensive phase of the LDE experiment, are subsampled from 100 to 3000 m depth and are used as the population space for evaluation. The 100 m limit is near the seasonal thermocline (Fig. 1a) and the 3000 m limit is approximately the depth of the shallowest CTD cast.

2. Methodology

The optimal estimate of a linear operation on a random variable equals that linear operation on the optimal estimate of the same random variable (see Bretherton et al. 1976). Operationally, potential temperature profiles are estimated first and then the derivative operator is approximated by a discrete model for differentiating the optimally estimated data. Ideally, the optimal estimate of the vertical derivative of potential temperature should be both unbiased and have minimum variance. The bias and standard deviation properties of common models of the vertical derivative of potential temperature are presented as a function of estimation interval.

a. Filtering

The first step is to optimally estimate potential temperature. For mesoscale processes, hydrographic sampling is dense (e.g., Gandin 1965) in the vertical, hence a simple scheme for estimating potential temperature profiles will suffice. The choice here is to low-pass filter the hydrographic profiles to remove submesoscale noise. Since the scale of interest is much greater than 100 m and the scale of the noise is typically less than 100 m, the estimation scheme chosen to interpolate potential temperature profiles is to filter the data with a Gaussian filter such that 99% of the variance is removed on scales of less than 100 m. This strict requirement forces a large filter footprint that can not be avoided with any filtering technique (see the discussion by Thompson 1983 in the context of filtering time series).

To meet the specified response at the cutoff wavenumber, a Gaussian filter requires 115 points (285 m for data spaced every 2.5 m) positioned symmetrically about the point to be filtered. However, the profiles are not stationary in the vertical, even in the weak sense, as can be seen in Fig. 1. To prevent biases in the filtered profiles, the profiles must be detrended before filtering. The mean potential temperature profile could be used to detrend the data before filtering. Since the acquisition of such a large number of profiles for calculating a good mean profile is a rare event in oceanography, a trend calculated for each profile is tested. The usual method of detrending a dataset is to fit a straight line by least squares. But with hydrographic data, the trend is not linear in the main thermocline and the trend changes below the thermocline. Due to the depth dependent trend, the use of a variable knot cubic spline (de Boor 1978) fitted to each profile is tested as an

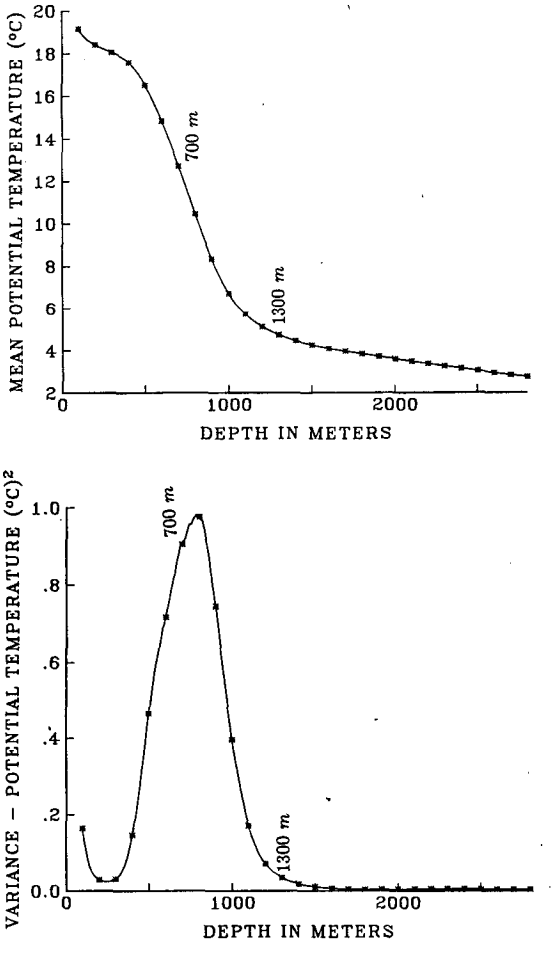

FIG. 1. (a) Mean potential temperature as a function of depth, calculated from 543 LDE CTD drops. Asterisks are at every 100 m in the vertical, starting at a depth of 100 m, to aid the reader in following the discussion in the text. (b) Variance of potential temperature as a function of depth.

alternative to using the LDE mean temperature curve (Fig. 1a) for detrending the data. Mariano (1986, hereafter M86) demonstrated that a three knot cubic spline, with the middle knot between 1050 and 1300 m, is the best variable knot cubic spline for detrending hydrographic data before filtering and that the vertical derivative estimates using a variable knot cubic spline to model the dependency of potential temperature with depth was inferior to the models described next.

b. *Vertical derivative models*

Three of the most common models for estimating first derivatives are tested on n data points (z_i, θ_i) from oceanic hydrographic data. The θ_i is potential temperature at depth z_i. The variable parameter n is an odd positive integer that determines the estimation interval. The resolution of the data points is 2.5 m, the vertical spacing of the archived CTD data from the LDE.

The first model is a simple finite difference which uses only two of the n data points,

$$\frac{\partial\theta}{\partial z} = \frac{\theta(z_n) - \theta(z_1)}{z_n - z_1}. \tag{2.1}$$

For all the derivative models, the value of the derivative is implied at the middle data point, z_0.

The second model tested, since it is frequently assumed in analytic studies, is

$$\theta(z_i) = b_1 \exp(-b_2 * z_i), \quad i = 1, 2, \cdots, n, \tag{2.2}$$

which after taking the natural logarithm of both sides becomes a linear least-squares problem. The regression coefficients b_1 and b_2 are estimated using the n data points and the resulting exponential function is differentiated with respect to z and evaluated at the point of interest, z_0, viz.

$$\frac{\partial\theta}{\partial z} = -b_2 b_1 \exp(-b_2 * z_0). \tag{2.3}$$

The third model is a mth order Taylor polynomial

$$\theta(z_i) = \theta(z_0) + b_1 * (z_i - z_0) + \cdots + \frac{b_m * (z_i - z_0)^m}{m!}, \tag{2.4}$$

where the regression coefficient b_j is the jth derivative. First, second, and third order Taylor polynomials are tested. This model reduces to model number one for $m = 1$ and for two data points.

The choice of derivative model and digital filter should be made in tandem. For instance, Miller and Evans (1985) has shown that a Butterworth low-pass filter must be designed to eliminate the undesirable response of the finite difference vertical derivative model at high wavenumber. They showed that as you increase the estimation interval, the amount of smoothing should also be increased. The matching of filter response and the response of your approximate differentiator is crucial for estimating mean gradients from individual hydrocasts.

c. *The error model*

There are 543 estimates of the vertical derivative at 700 and 1300 m for each estimation model and estimation interval tested. For a given interval and model, the 543 estimates of vertical derivatives will not be the same due to their stochastic nature. The differences are due to natural variations of the vertical derivative (which are dynamically important on synoptic time scales) in space/time, submesoscale noise and estimation error.

Estimation error is subdivided into measurement and fitting errors. Measurement error includes the effect of digitization on a 2.5 m scale (i.e., subgrid scale noise) and sensor error. Fitting error is defined here to include the error due to approximation of the derivative operator by a discrete method and possible model error resulting from the wrong choice of the functional dependence of θ on z. Submesoscale noise is defined here as variations in temperature on scales between the resolved scale (a few meters) and the mesoscale (a few hundred meters).

The observed temperature (subscript 0) is defined as

$$\theta_0(x, y, z, t) = \theta_m(z) + \theta_e(x, y, z, t) + \theta_n(x, y, z, t), \tag{2.5}$$

the subscript m is for the sample mean, which for this study is a longitude/latitude/time arithmetic mean of the 543 estimated values at 700 and 1300 m. The second term on the right-hand side (rhs) of (2.5) is the dynamically important mesoscale perturbation of the mean field (subscript e for eddy). The third term on the rhs of (2.5) is the combined effect of measurement, fitting and submesoscale noise (subscript n). A vertical derivative estimate (est.) then can be expressed as

$$\left(\frac{\partial\theta}{\partial z}\right)_{\text{est.}} = \left(\frac{\partial\theta}{\partial z}\right)_m + \left(\frac{\partial\theta}{\partial z}\right)_e + \left(\frac{\partial\theta}{\partial z}\right)_n, \tag{2.6}$$

where the mean is just a function of z for a fixed estimation interval.

The variance of this estimate for a fixed estimation interval is

$$S^2_{\text{est.}} = S^2_{\partial\theta/\partial z|_e} + S^2_{\partial\theta/\partial z|_n}, \tag{2.7}$$

assuming a zero covariance term. The first term on the rhs of (2.7) is the natural variation of the derivative. The *best* estimator should minimize the second term on the rhs of (2.7) (or its square root); the variance (or standard deviation) that results from the combined effect of measurement, submesoscale and fitting error. The *best* estimator should also be unbiased, i.e. the

expected value of the estimator equals the expected value of the population being sampled. It is well known in the statistical literature (e.g., Seebur 1977), that for most estimators, both of these criteria can not be met simultaneously.

3. Bias and standard deviation curves of the vertical derivative models

The LDE mean $\partial\theta/\partial z$ curves (Figs. 2 and 4) and the standard deviation curves (Figs. 3 and 5) at depths 700 and 1300 m are estimated using the three models. The standard deviations are calculated in the usual fashion:

$$S_Q = \left[\frac{\sum_{i=1}^{np} (Q(i) - Q_m)^2}{(np-1)} \right]^{1/2}, \qquad (3.1)$$

where $Q(i)$ is either the 700 or 1300 m $\partial\theta/\partial z$ estimate from the ith CTD drop and np is 543. Not all possible combinations of filtering type and functional forms are tested. The reason for this and the lack of resolution in some of the estimation intervals is due to large computational time required for these calculations and that their inclusion does not change any of the results of this study. The ten combinations tested in this study are: 1) a finite difference (FD) of unfiltered potential temperature data; 2) a FD of filtered data that was detrended with the LDE mean potential temperature curve (Fig. 1a); 3) a FD of filtered data that was detrended with a cubic spline fit to the entire subsampled profile (100 m to 3000 m); 4) a straight line regression (SL) of unfiltered data; 5) a quadratic polynomial regression (QP) of unfiltered data; 6) a QP of filtered data that was detrended with the LDE mean potential temperature curve; 7) a QP of filtered data that was detrended with a cubic spline fit; 8) an exponential regression (EX) of filtered data that was detrended with the LDE mean potential temperature curve; 9) an EX of filtered data that was detrended with a cubic spline fit; and 10) a cubic polynomial regression (CP) of unfiltered data.

The behavior of these curves as a function of estimation interval for the different models is discussed below. It is shown that the behavior of the mean curves is determined by the magnitude of the estimands' (i.e., the data points in a given estimation interval) vertical derivative. The behavior of the standard deviation curves is determined by the number and variance of the estimands. The differences between the 700 and 1300 m curves are due to $\partial\theta/\partial z$ being a maximum in more or less symmetric temperature profile, whereas at 1300 m, $\partial\theta/\partial z$ is rapidly decreasing with depth.

a. The 700 m bias and standard deviation curves

The ten different estimation combinations cluster about a mean of 0.0213°C m^{-1} for estimation intervals less than 200 m (Fig. 2). This value is used as the true mean at 700 m. For estimation intervals above 200 m, the models diverge. By 600 m there are three groupings, the finite difference models (FD) are in group one, the straight line (SL), quadratic polynomial (QP), and exponential (EX) regressions are in the second group, the cubic polynomial regression (CP) is alone in the third group. The trend at 600 m continues as these estimates monotonically decrease to about 1200 m. At 1200 m, the mean of the FD group 1 is 0.0125°C m^{-1}, the mean of the QP, SL, and EX group 2 is 0.014°C m^{-1} and the CP group 3 has a mean of 0.020°C m^{-1}. There is a hint of this trend changing at 1200 m for the FD models (group 1).

The behavior of the 700 m bias curve can be explained easily by using the mean and variance curves of Fig. 1. The 700 m bias curve (Fig. 2) decreases as the estimation interval increases because the estimands' vertical derivatives of potential temperature are smaller than the vertical derivative of potential temperature at 700 m. For instance when the estimation interval is 600 m, data from 400 to 1000 m is used to estimate the derivative at 700 m. The vertical derivatives of potential temperature at 400 and 1000 m are less than

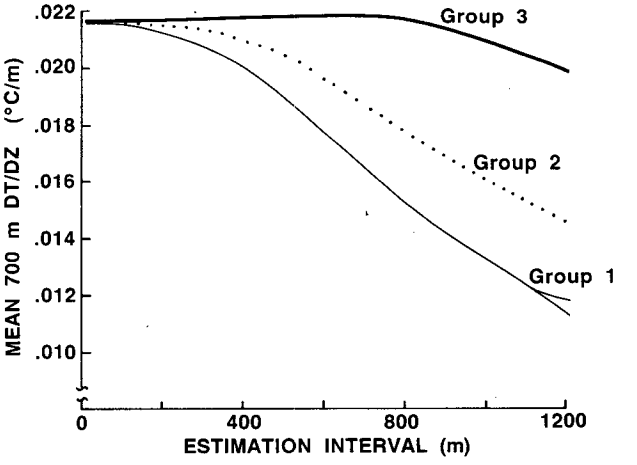

FIG. 2. The mean vertical derivative of potential temperature at 700 m as a function of estimation interval. The 10 combinations tested in this study are placed into three groups. Group 1 consists of a finite difference (FD) of unfiltered potential temperature data, a FD of filtered data that was detrended with the LDE mean potential temperature curve (Fig. 1a), and a FD of filtered data that was detrended with a cubic spline fit to the entire subsampled profile (100 m to 3000 m). Group 2 consists of a straight line regression (SL) to unfiltered data, a quadratic polynomial regression (QP) to unfiltered data, a QP to filtered data that was detrended with the LDE mean potential temperature curve, a QP to filtered data that was detrended with a cubic spline, an exponential regression (EX) to filtered data that was detrended with the LDE mean potential temperature curve, and an EX to filtered data that was detrended with a cubic spline. Group 3 consists of a cubic polynomial regression (CP) to unfiltered data. Unless otherwise stated for Figs. 2–6, the estimates in each group cluster tightly about each plotted curve and while some information is lost due to this grouping the curves are a lot more readable.

the vertical derivative at 700 m. As the estimation interval increases, more and more estimands are used whose vertical derivatives are less than at 700 m. This leads to the situation shown in Fig. 2, i.e., as the estimation interval increases, the vertical derivative estimates for 700 m become biased lower and lower, due to using biased estimands. The trend starts to change at an estimation interval of 1200 m, since now one is using estimands near 100 m, whose vertical derivatives have a relatively larger magnitude due to the seasonal thermocline.

The standard deviations shown in Fig. 3 almost all (except group 3) converge to a value of 0.0005°C m^{-1} at an estimation interval of 1200 m. Just before 1200 m, some of the standard deviations start to increase slightly. The decrease of the standard deviation as the estimation interval increases is expected for the regression models since more and more data points are being used. The decrease for the finite difference model (group 1) is due to the denominator of (2.1) dominating over the numerator for the larger estimation intervals. The slight increase seen near the 1200 m estimation interval is due to the use of data points whose variance is locally larger (Fig. 1b). The standard deviation of group 3 exhibits very different behavior from that of the other estimates. The reason for this is given after discussion of the 1300 m curves.

Regardless of whether the mean LDE profile or a spline fit to every profile was used for detrending, all the estimators which used filtered potential temperature profiles converge to a value of 0.0017°C m^{-1} (Fig. 3) as the estimation interval decreases to zero. By inspecting the entire 700 m (and 1300 m) bias and standard deviation curves, it is clear that a cubic spline fit can be used as a proxy to a mean curve for detrending hydrographic profiles before filtering.

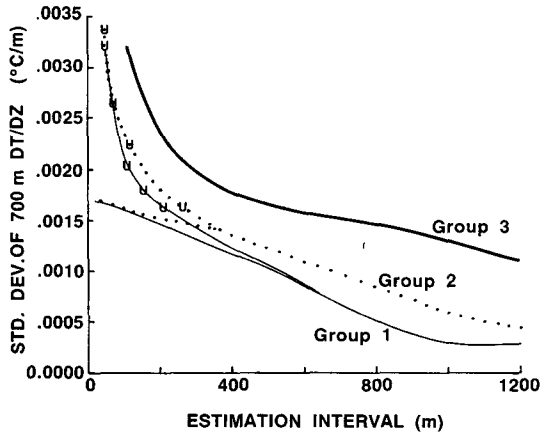

FIG. 3. The standard deviations of the vertical derivative estimates at 700 m as a function of estimation interval. The groups are explained in Fig. 2 and in the text. "U" denotes vertical derivative estimates using unfiltered data.

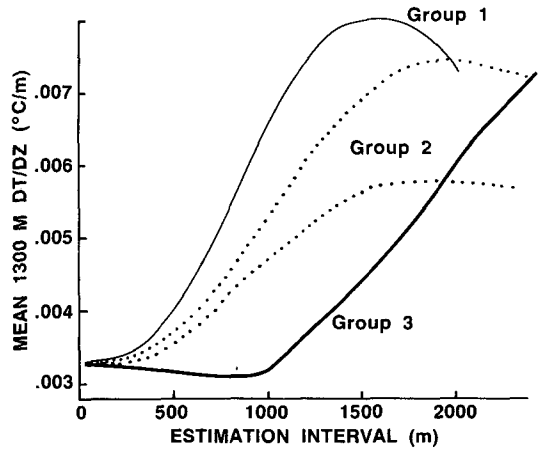

FIG. 4. As in Fig. 2, but for 1300 m. The lower branch of the group 2 curve is for vertical derivative estimates using an exponential regression.

b. The 1300 m bias and standard deviation curves

The mean value of the derivative at 1300 m is 0.0032°C m^{-1} for estimation intervals up to 200 m for all the methods tested. This value is used as the true mean at 1300 m. The 1300 m mean curves (Fig. 4) show the same tendency of the FD grouping together, the anomalous behavior of the CP model (group 3), and the SL and QP models grouping together but now the EX model diverges from the second group and forms the lower branch of the group 2 curve. The mean 1300 m curve starts at a value of 0.0032°C m^{-1} and increases with group 1 exhibiting the largest derivative estimates.

The same argument used for the behavior of the 700 m mean curves is used at 1300 m, but as the estimation interval increases, estimands are used that have a larger derivative than the derivative at 1300 m; hence the 1300 m estimate is biased on the high side. The upward trend in Fig. 4 starts to level off as the estimation interval reaches 1500 m. This leveling off is due to the influence of 18°C water, whose vertical derivative is a local minimum (Worthington 1959). The influence of 18°C water can be most clearly seen in the FD models (group 1) as the estimation interval becomes 2000 m.

For the 1300 m standard deviation curve, there are the same three distinct groupings with the EX model diverging from group 2 in the estimation interval from 500 to 2000 m. The models using unfiltered data (denoted by U) are noisier than the models using filtered data for small estimation intervals, which is also true for the 700 m derivative estimates (Fig. 3). Again the CP derivative estimates are noisier at larger estimation intervals and show less variation in the mean up to an estimation interval of 1000 m. The local maximum in the 1300 m standard deviation curves (Fig. 5) is due to the use of estimands that have more variance (see Fig. 1b). For instance at an estimation interval of 400

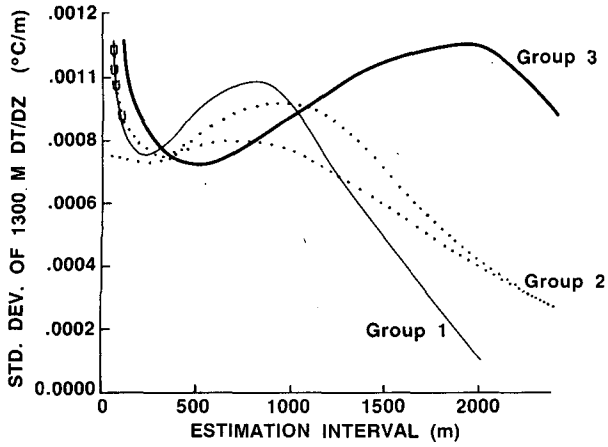

FIG. 5. As in Fig. 3, but for 1300 m. The lower branch of the group 2 curve is for vertical derivative estimates using an exponential regression.

m, one uses potential temperature data from 1100 to 1500 m. As the estimation interval increases, more and more estimands are used that have larger and larger variance; this offsets the decrease expected in the standard deviation curves due to using more and more points. The standard deviation curves start to decrease again beyond an estimation interval of 1000 m (800–1800 m), which is outside the window of large variances and the effect of using more and more data points dominates again.

For estimation intervals greater than 1000 m, the most rapid decrease in the standard deviation of the 1300 m derivative estimates is for the FD models (group 1). This estimate depends on only two points, which both have a small variance at large estimation interval. This fact and the smoothing effect of the denominator in the finite difference cause this rapid decrease, but there is a corresponding large positive bias.

c. *Discussion of the bias and standard curves*

Four distinct patterns emerge from the mean and standard deviation curves of the vertical derivative models; 1) The convergence of all the models as the estimation interval goes to zero and the convergence of the individual models at a fixed estimation interval, 2) the relative placement of the groups is the same in the 700 m and 1300 m standard deviation curves, 3) there is no difference between the type of filtering or whether filtering was done at all for large estimation intervals, and 4) there is a bias-variance tradeoff for all the models tested.

The convergence of all the models as the estimation interval goes to zero and the convergence of the individual models at a fixed estimation length is due to the large sample size. One needs only to assume about 100 degrees of freedom from the 543 profiles and use the law of large numbers to easily prove the observed convergences.

The grouping of models is determined by the number of *significant* parameters to be estimated and hence is independent of z_0. For example, when estimating the vertical derivative at 700 m using the Taylor polynomials (2.4), the contribution to the estimate of θ at an estimation interval of 1000 m for a polynomial fit is such that the $\theta(z_0)$ term and the first derivative term of (2.4) are the same order of magnitude [i.e., $\theta(z_0)$ is the same order of magnitude as $(\partial\theta/\partial z)*(z - z_0)$]. The magnitude of the quadratic term is an order of magnitude smaller (determined from 543 estimates), but the cubic term is the same order of magnitude as $\theta(z_0)$ and the first derivative term. The group consisting of SL, QP and EX models have only two significant parameters to estimate. Since the contribution to the regression fit by the second derivative term at a large estimation interval is small, the second derivative term does not help the QP model to fit the estimands farthest from $\theta(z_0)$. In turn, these *distant* estimands must be accounted for by the zero and first order terms when less than a cubic polynomial fit is used, hence the SL, QP, and EX models have similar bias characteristics. The CP model does not exhibit the same bias tendencies as the other models for estimation intervals up to 1000 m because it has one more significant parameter, the third derivative term, which is the same order of magnitude as the $\theta(z_0)$ term and the first derivative term of (2.4). Thus, as the estimation interval increases, the CP model can better fit the *distant* (from z_0) estimands and these *distant* estimands have less of an effect on the derivative estimate at z_0. The price to pay for the lack of bias for the CP regression is the increased variance, which results from the use of more parameters.

The standard deviation curves (Figs. 3 and 5) clearly show the effect of smoothing the data. The models using the unfiltered data (U) exhibit large standard deviations for estimation intervals under 200 m. It will be shown below that the large standard deviations are due to measurement and submesoscale noise. For estimation intervals less than 200 m, the data must be smoothed in the fashion described by Miller and Evans (1985) and discussed above. The models using a large estimation interval inherently smooth the derivative estimate themselves.

Beyond an estimation interval of 200 m, the estimated means are mostly biased low at 700 m and biased high at 1300 m. Unfortunately, the models and estimation intervals tested show that the estimates with the lowest standard deviations (equivalently, the lowest variances) are the most biased. An *optimal* estimator in the classic sense does not exist and some other criterion of merit must be defined for the problem at hand.

Analogous results are seen in the estimation of the vertical derivatives of potential density. The only difference, of course, is that density is a decreasing func-

tion of different magnitude. The mean vertical derivative of density at 700 m is -0.0023 (g cm^{-3})/m. The mean vertical derivative of density at 1300 m is -0.0003 (g cm^{-3})/m.

4. The vortex stretching estimates

Since there is a variance-bias trade-off, some other criterion of merit needs to be defined for estimating mesoscale vertical derivatives of potential temperature and density. The problem at hand is the estimation of the vortex stretching using hydrographic and SOFAR float data. It is proposed that vortex stretching calculated from our *best* estimator of the vertical derivative of potential temperature and density should be both robust to small changes in the estimation interval and not significantly different from the independent vortex stretching estimates of MR89. In that study, vortex stretching was calculated as the residual in the Lagrangian vorticity balance,

$$\frac{df}{dt} + \frac{d\zeta}{dt} + \text{vortex stretching} = 0. \qquad (4.1)$$

The material time derivatives of the planetary vorticity (f) and the relative vorticity (ζ) were calculated using clusters of SOFAR floats to tag water parcels. The error in the residual method (4.1) for estimating vortex stretching is 0.4×10^{-12} s^{-2} (MR89).

a. *The methodology for the vortex stretching estimates*

The data available consist only of pairs of hydrocasts near float trajectories, so the time derivative of (1.1) is a simple finite difference in time, and f, the planetary vorticity, is the average of the 2 values of f at the CTD/STD locations. If the bias error in the estimate of $\partial\theta/\partial z$ or $\partial\rho/\partial z$ is constant from one hydrocast to the next, the finite difference in time would remove the entire bias error. Then one may take advantage of a large estimation interval with its low standard deviation. But the biases themselves are statistical quantities that vary, so we are forced to test the various vertical derivative estimates and see which estimate is the best for estimating vortex stretching.

Four vortex stretching estimates are shown in Fig. 6 as a function of estimation intervals for three typical hydrographic pairs: (a) 34, 54; (b) 20, 40; and (c) 23, 42 along float trajectories 84, 64, and 62, respectively (Fig. 7). The four vortex stretching estimates use FD, SL, QP and CP regressions to unfiltered density profiles for calculating the vertical derivatives. Similar vortex stretching estimates for STD hydrographic pairs: (24, 44), (21, 41), (21, 42), (34, 54), (22, 44), (4, 35) and LDE CTD pairs (5, 56), (12, 56), (13, 56), (385, 404), (14, 58), (58, 129), (17, 41), (17, 42) and (120, 134) are not shown. Estimates below the 400 m estimation interval are not shown since those estimates fluctuate wildly. One can get a feel for this fluctuation by focusing on the four estimates (when they are not off scale) in the neighborhood of the 400 m estimation interval (Fig. 6).

The two vortex stretching estimates based on a QP and FD derivative model fluctuate the most. Estimation intervals from 600 to 1000 m exhibit the least fluctuations for all the models tested. The models and estimation intervals that are most robust are clearly the SL and CP models from 600 to 1000 m. For these models and estimation intervals, the vortex stretching estimates for temperature and density agree quite well (M86).

b. *Comparison of vortex stretching estimates*

Since the *best* estimation interval can not be distinguished, regressions of lengths 700, 800 and 900 m are

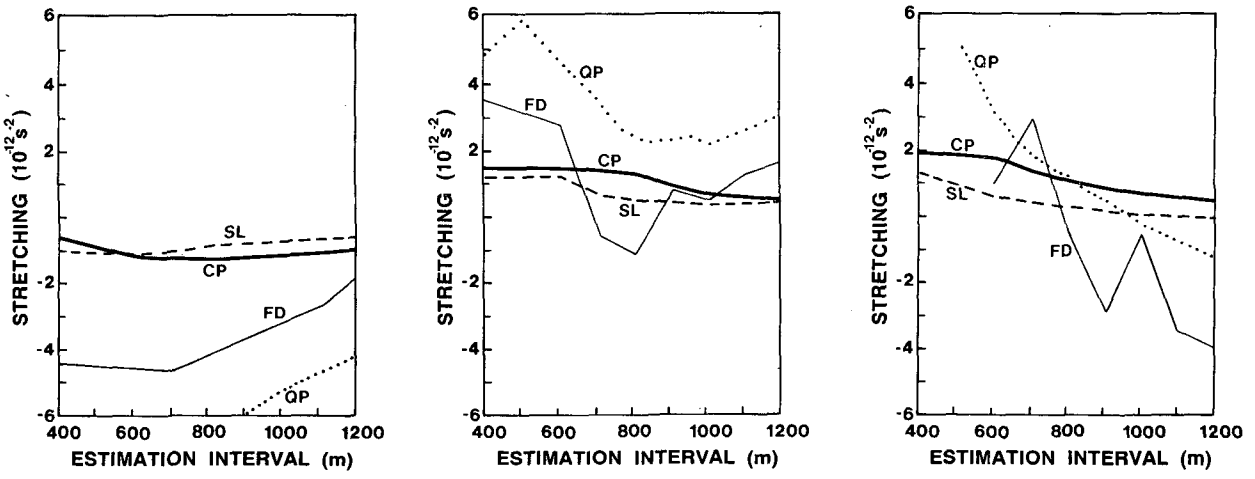

FIG. 6. Vortex stretching estimates for three 700 m floats (84, 64, 62) and hydrographic pairs (a) 34, 54; (b) 20, 40; (c) 23, 42, respectively, as a function of estimation interval for the following mesoscale vertical derivative models and unfiltered hydrographic data: 1) a finite difference (FD) of potential density data, 2) a straight line regression (SL) of potential density data, 3) a quadratic polynomial regression (QP) of potential density data, and 4) a cubic polynomial regression (CP) of potential density data.

averaged to calculate vortex stretching for comparison with independent vortex stretching estimates based on the residual method (4.1) for three float groups (Table 1). The vortex stretching estimates based on the residual method uses float clusters from MR89. The first float group is from the *Gyre* cruise (Fig. 7a), which was specifically designed to estimate vortex stretching using a Lagrangian approach. The next two float groups in Table 1 are lucky byproducts of the Eulerian CTD sampling strategy (Fig. 7b).

Using the residual method for floats (62, 64, 66, 67, 89), vortex stretching is estimated to be 1.02×10^{-12} s^{-2} and for floats (62, 64–69, 89) we estimate $0.95 \times 10^{-12}\,s^{-2}$. (The first estimate uses the floats that best correspond with the STD hydrocasts and the second estimate uses the floats determined by M88's cluster selection criteria.) The vortex stretching estimate that uses a CP regression to estimate the vertical derivative of density agrees well with the residual estimates for the first three hydrographic pairs (Table 1), which are near the centroid of the float cluster (Fig. 7a). The lack of agreement for the fourth pair of the first group is probably because the residual estimates are representative of the centroid of the float cluster and the fourth pair of hydrographic stations is on the perimeter of the float cluster (Fig. 7a).

The best agreement with the residual method for the second float group is the vortex stretching estimate that uses a CP regression to estimate the vertical derivative of density for CTD pair 385, 404, following float 53 (Table 1). The anomalous vortex stretching estimates for float 60 are due to asynoptic estimation periods. The residual method uses float data (53, 59, 60) from days 3642–3672, float 60 vortex stretching estimates uses hydrocasts from days 3650 and 3655. (Note that float 53 vortex stretching estimates uses hydrocasts from days 3669 and 3672). Mariano and Rossby extrapolated the residual method's vortex stretching time series and estimated the stretching on day 3652 to be 0.45×10^{-12}, which is in close agreement with the vortex stretching estimate that uses a CP regression to density (Table 1).

For float group three, the vortex stretching estimate based on a CP regression to density is the closest to the residual vortex stretching estimate (Table 1). The differences in magnitude are attributed to a combination of estimation noise and a sharp decrease in stretching for float cluster (54–56, 61) after day 3653.

It is not possible to accurately estimate the vortex stretching with the models tested in this study at 1300 m. The *Gyre* STD data was tested using estimation intervals ranging from 100 to a maximum 400 m (the deepest STD cast is 1500 m). The stretching estimates from the *Gyre* STD data are all at least an order of magnitude larger than the estimates of MR89, despite good pairs of hydrocasts following the floats. The 1300 m results using the LDE CTD data are more discouraging. There are ninety-eight times when a hydrocast and a float are within one-half of a day and 10 km of each other in the E–W and N–S direction at least twice following a float. Ninety-eight percent of the 1300 m vortex stretching estimates calculated using SL, QP, CP, and FD and estimation intervals of 200 to 2000 m are one to two orders of magnitude too large.

Stretching can not be estimated at 1300 m due to a low signal-to-noise ratio. The standard deviation due to noise at 1300 m is twice that of S_n at 700 m. This noise at 1300 m is amplified relative to 700 m, by the order of magnitude smaller mean derivative at 1300 m [look ahead to (4.4)]. Physically, the magnitude of w is a maximum at 1300 m (Rossby et al. 1986); hence the stretching, $-f(\partial w/\partial z)$, is expected to be small.

c. *Analysis of vortex stretching error*

Measurement error (me), submesoscale error and fitting error contribute to $S_{\partial\theta/\partial z_n}$, the vertical derivative estimation error. The fitting error's contribution is determined by calculating the root-mean-square difference between the data and estimates predicted by the models and is much smaller $O(10^{-5})$ than the contributions due to submesoscale and measurement errors.

Since our Gaussian filtering scheme removes 99% of the submesoscale and measurement variance on

TABLE 1. Vortex stretching estimates (10^{-12} s^{-2}) for 700 m.

Float group	CTD/STD		SL		CP		Residual method
	Pair	Time	Density	Temperature	Density	Temperature	
62	21, 42	3727–3731	0.66	0.28	1.01	0.02	
62	23, 42	3727–3731	0.17	0.30	0.97	1.03	1.02
64	20, 40	3727–3731	0.41	0.35	1.07	0.94	0.95
67	19, 39	3727–3730	−0.67	−0.76	−1.51	−1.11	
60	17, 41	3650–3655	0.52	0.52	0.79	0.72	
60	17, 42	3650–3655	−0.17	−0.28	0.41	0.19	−.56
53	385, 404	3669–3672	−0.08	−0.12	−0.35	−0.32	
54	5, 56	3649–3657	−0.31	−0.17	−0.88	−0.53	
55	13, 56	3650–3657	−0.63	−0.58	−1.23	0.95	−2.05
55	12, 56	3650–3657	−0.31	−0.37	−0.85	−0.69	

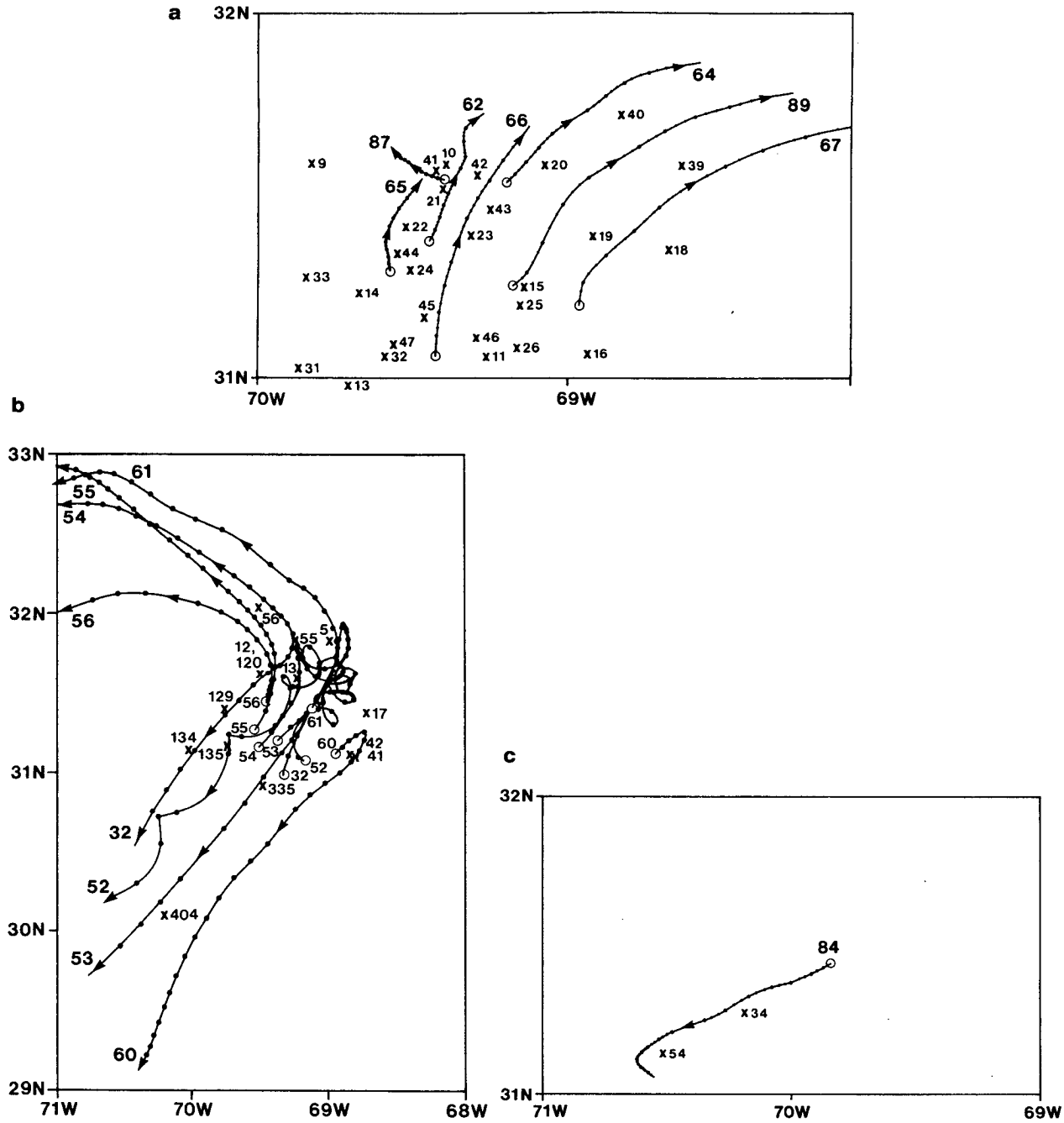

FIG. 7. (a) Trajectories of 700 m floats launched (open circles) in the LDE region. Time interval is in Julian day. Fixes are every 8 hours. The larger dots are at daily intervals. The float number is given near the end of the trajectory. The numbered Xs are the STD hydrocasts from *Gyre* cruise G-6-78. Most of the hydrocasts are from truncated Julian days 3727–3732. (b) As in (a) but for CTDs from the LDE intensive survey that by luck follow float trajectories. All vortex stretching estimates using hydrographic pairs separated by less than 2 days were an order of magnitude too large. (c) As in (a) but for trajectory of float 84 from 3723–3737.

scales less than 100 m, the total contribution by submesoscale and measurement error to $S_{\partial\theta/\partial z_n}$ can be estimated as the difference in the standard deviation (3.1) of the estimates from the unfiltered data and the estimates from the filtered data at a given estimation interval. The individual contributions of submesoscale and measurement error are decoupled by estimating the contribution of measurement error.

Here $S_{\partial\theta/\partial z|_{me}}$, the contribution of measurement error in estimating the vertical derivative using a FD of

length $z_2 - z_1$, is easily derived using propagation of errors to be

$$S_{\partial\theta/\partial z|_{me}} = \frac{2S_{\theta_{me}}}{(z_2 - z_1)}. \quad (4.2)$$

Theoretically, $S_{\theta_{me}}$ is calculated by extrapolating the estimated structure function, $\hat{F}(z_j - z_i)$, to zero (Gandin 1967) and using the relationship,

$$2S^2_{\theta_{me}} = \hat{F}(0). \quad (4.3)$$

The true structure function is defined as

$$F(z_j - z_i) = \overline{[\theta(z_j) - \theta(z_i)]^2}.$$

We must use $\hat{F}$, rather than F, since we do not know the true $\theta(z)$. The large curvature of F near $F(0)$ and estimation noise limit the practicality of extrapolating $\hat{F}$ to zero (op. cit. and M86).

The $S_{\theta_{me}}$ is estimated to be 0.02°C from a cubic polynomial fit about the third data point of $\hat{F}$ (M86). Bryden (1976) estimated 0.01°C using temperature sensors that were close (6 to 1600 m) in the horizontal. The measurement error is assumed to be 0.015°C, an average of the two independent estimates.

Table 2 lists the standard deviations of the 700 m FD vertical derivative estimate for the unfiltered and filtered temperature data from the 543 CTD LDE drops. Contributions by measurement and submesoscale error to the vertical derivative estimation error are about equal for an estimation interval of 40 m. For estimation intervals greater than 200 m, the submesoscale error contribution (2×10^{-5} °C) is an order of magnitude less than the measurement error contribution (15×10^{-5} °C). Thus, $S_{\partial\theta/\partial z|_n}$ is well approximated by $S_{\partial\theta/\partial z|_{me}}$ (4.2).

Using propagation of errors with data from times t_1 and t_2, the standard deviation for vortex stretching estimation due to measurement error in estimating the vertical derivative is

$$S_{fd/dt[\ln(\partial\theta/\partial z)]} = \frac{2fS_{\partial\theta/\partial z|_{me}}}{[(t_2 - t_1)\,|\,\partial\theta/\partial z\,|\,]}. \quad (4.4)$$

For example, if d/dt is typically 4 days, f is 0.76×10^{-4} s^{-1} and an order of magnitude stretching estimate is 10^{-12} s^{-2}, using a FD vertical derivative requires an estimation interval of 650 m. It is not possible to obtain an accuracy of 10^{-13} s^{-2} (i.e., 10% of the signal) with the FD vertical derivative and hence the FD vortex stretching estimates fluctuate wildly (Fig. 6).

TABLE 2. Standard deviations of the finite difference method (10^{-2} °C)

Estimation interval (m)	Unfiltered	Filtered	Unfiltered minus Filtered	Measurement	Submesoscale
40	0.315	0.164	0.151	0.08	0.071
100	0.200	0.157	0.043	0.03	0.013
200	0.159	0.142	0.017	0.015	0.002
400	0.118	0.112	0.006	0.008	0.000
800	0.045	0.045	0.000	0.004	0.000
1000	0.024	0.025	0.001	0.002	0.000
1200	0.031	0.026	−0.005	0.001	0.000

For the polynomial fit (2.4) $S_{\partial\theta/\partial z|_{me}}$ is given by

$$S_{\partial\theta/\partial z|_{me}} = (\mathbf{R}^T\mathbf{R})^{-1} S_{\theta_{me}}, \quad (4.5)$$

where

$$\mathbf{R} = \begin{pmatrix} 1 & (z_1 - z_0) & \dfrac{(z_1 - z_0)^m}{m!} \\ 1 & (z_2 - z_0) & \dfrac{(z_2 - z_0)^m}{m!} \\ & \vdots & \\ 1 & (z_n - z_0) & \dfrac{(z_n - z_0)^m}{m!} \end{pmatrix}.$$

(4.5) assumes that the mth order polynomial regression is the true model (see Seebur 1977). By substituting (4.5) into (4.4) and assuming the same f, $t_2 - t_1$, $S_{\theta_{me}}$ and $\partial\theta/\partial z$ as before, it is easily shown that to reduce the vortex stretching error to 10^{-13} s^{-2} requires an estimation interval of about 700 m, which agrees with Fig. 6.

5. Summary

None of the vertical derivative models tested are both unbiased and minimum variance. The proposed criterion of merit is that the *best* method is robust with respect to a change in estimation length for estimating vortex stretching and gives vortex stretching estimates that are not significantly different from the independent vortex stretching estimates of MR89. For the case discussed in section 4, the *best* estimator of vortex stretching is a cubic polynomial fit of length 700 to 900 m to the density data at 700 m. Vortex stretching can not be estimated using the time rate of change of the vertical derivative of density or temperature following float clusters at 1300 m with any of the vertical derivative models tested due to a low signal-to-noise ratio, thus vortex stretching estimates using this approach should not be made where $\partial w/\partial z$ is small.

Due to the remarkable similarity of vertical profiles of potential temperature and density below the seasonal thermocline, the bias and standard deviation curves given here will need little modification when estimating mesoscale vertical derivatives from other midlatitude hydrographic profiles. The standard deviation and bias curves can be used as a guide for estimating vertical derivatives given different criterion of merit. For example, if the design criterion is to estimate the vertical derivative of temperature at 700 m with the smallest

estimation error possible under a strong constraint of no bias, then Figs. 2 and 3 suggest that the data should be filtered, the estimation interval should be on the order of 150 m and a least-square straight line regression will suffice.

How robust are these results for hydrographic profiles from other regions of the world's oceans? The most robust result is that the mesoscale derivatives should be estimated using a range of data whose derivative values are not significantly different from the derivative at the point of estimation. This implies that for calculating quantities involving vertical gradients (e.g., the Brunt-Väisälä frequency), the estimation interval should be variable with respect to depth in the water column and station location. For instance, the estimation interval for 18°C water would be much smaller than the estimation interval for North Atlantic Deep Water, which is at a nominal depth of 2500 m in Fig. 1a. Also, the "best" estimation interval would be dictated by the particular feature (e.g., rings, submesoscale coherent vortices, fronts) sampled by a profile. As discussed by Mariano (1990), it is worth the extra effort to tailor the estimation scheme for particular cases based on features evident in the data. Thus, the results presented herein, provide guidelines that can be applied to a wide variety of contexts.

Acknowledgments. This work formed one portion of the author's doctoral dissertation at the University of Rhode Island. It is a pleasure to acknowledge the guidance and support provided by Professor Tom Rossby. The collection, processing and initial analysis of the SOFAR float data was generously supported by the National Science Foundation under Grant OCE78-18662-A02. The preparation of this manuscript was supported by the Office of Naval Research Contract N00014-84-C-0461 and Institute for Naval Oceanography contract S8766 at Harvard University. The final preparation of this manuscript was done while the author was supported by the Rosenstiel Fellowship at RSMAS, University of Miami. The author expresses his appreciation to Professor Mark Wimbush, Mr. Jerry Miller, and an anoymous reviewer for their suggestions and to Dr. Eric Lindstrom for his assistance in acquiring the LDE CTD dataset.

REFERENCES

Bryden, H. L., 1976: Momentum, mass, heat, and vorticity balances from oceanic measurements. Ph.D. thesis, MIT-WHOI Joint Program in Physical Oceanography, 127 pp.

Bretherton, F. P., R. E. Davis and C. B. Fandry, 1976: A technique for objective analysis and design of oceanographic experiments applied to MODE-73. *Deep-Sea Res.*, **23**, 559–582.

de Boor, C., 1978: *A Practical Guide to Splines.* Springer-Verlag, 392 pp.

Gandin, L. S., 1965: *Objective Analysis of Meteorological Fields,* Israel Program for Scientific Translations, 242 pp.

Mariano, A. J., 1986: On the estimation of first order dynamical quantities in the Lagrangian potential vorticity equation. Ph.D. thesis, University of Rhode Island, 166 pp.

——, and H. T. Rossby, 1989: The Lagrangian potential vorticity balance during POLYMODE. *J. Phys. Oceanogr.*, **19**(7), 927–939.

——, 1990: Contour Analysis: A new approach for melding geophysical fields. *J. Atmos. Oceanic Technol.*, in press.

Miller, J. L., and D. L. Evans, 1985: Density and Velocity Fine Structure Enhancement in Oceanic Eddies. *J. Geophys. Res.*, **90**(C3), 4793–4806.

Rossby, H. T., J. F. Price and D. Webb, 1986: The spatial and temporal evolution of a cluster of SOFAR floats in the POLYMODE Local Dynamic Experiment (LDE). *J. Phys. Oceanogr.*, **16**, 428–442.

Seebur, G. A. F., 1977: *Linear Regression Analysis.* Wiley & Sons, 456 pp.

Spain, D. L., R. M. O'Gara and H. T. Rossby, 1980: SOFAR Float Data Report of the POLYMODE Local Dynamics Experiment. Tech. Rep. 80-1, 200 pp. Graduate School of Oceanography, University of Rhode Island.

Thompson, R. O. R. Y., 1983: Low-pass filters to suppress inertial and tidal frequencies. *J. Phys. Oceanogr.*, **13**, 1077–1083.

Worthington, L. V., 1959: The 18° water in the Sargasso Sea. *Deep-Sea Res.*, **5**, 297–305.